Wave-Induced Local Steady Forces on a Column-Supported Very Large Floating Structure

Masashi Kashiwagi
Research Institute for Applied Mechanics, Kyushu University
Fukuoka, Japan

ABSTRACT

An accurate numerical calculation method is presented for the wave-induced steady forces and moments on each of the columns supporting a very large floating structure. The method is based on the direct integration of the pressure over the wetted surface of each column. First-order quantities needed in computing the pressure are determined by applying a higher-order boundary element method combined with the wave-interaction theory taking account of hydrodynamic interactions exactly within the linearized potential theory. The effects of motions of a structure are incorporated consistently up to second-order in the wave amplitude. Experiments in head waves are also conducted using 64 truncated vertical cylinders arranged in a periodic array of 4 rows and 16 columns. Steady wave forces are measured at 6 different positions among 64 cylinders, and they are all in good agreement with computed results. Some characteristics in the variation tendency of the local steady forces are summarized.

KEY WORDS: drift force and moment, hydrodynamic interactions, pressure-integration method, trapped mode

INTRODUCTION

A column-supported structure has been considered as a possible type of very large floating structures. This structure consists of a large number of floating columns which support a thin upper deck. By comparison with an alternative pontoon type which has been studied recently by many researchers (e.g. see Kashiwagi (1999) for a review), it is said that the column-supported type is advantageous in small motions in waves, because incident waves will transmit through a gap between columns.

However, this recognition may not be true. For instance, according to Maniar & Newman (1997), near-trapped modes among many cylinders occur at some critical frequencies and exert large wave forces on each cylinder of the array. Their study is based on a simple geometry, where a large number of bottom-mounted circular cylinders are periodically placed along a single straight line. Therefore no information is given on the near trapped-wave phenomena in a realistic array of columns and on the second-order wave drift force.

Recently, Kashiwagi (2000) presented a calculation method for the drift forces in the horizontal plane and the drift yaw moment on the basis of the momentum conservation principle. This method (referred to as the far-field method hereafter) is effective, because all necessary integrations over a control surface located far from the structure are analytically performed using Graf's addition theorem and Wronskian formulae for Bessel functions and the orthogonality of trigonometric functions to integrals in the circumferential direction. However, this method gives only the total force and moment acting on the structure.

Meanwhile, the steady drift forces can also be computed by integrating the pressure over the wetted surface of a structure and taking time average over a period. (Hereafter this method will be referred to as the pressure-integration method or the near-field method.) This pressure-integration method enables us to evaluate the local forces on each column, which is very useful in the analysis of structural strength and in the design of mooring systems. The present paper is concerned with this pressure-integration method.

The wave drift force is a second-order steady force with respect to the wave amplitude, which can be obtained from quadratic products of first-order quantities. In this paper, the boundary-value problems for the first-order velocity potentials are solved using Kagemoto & Yue's wave-interaction theory (1986) combined with a higher-order boundary element method (HOBEM). Thus, hydrodynamic interactions among many columns are taken into account exactly in the framework of the potential theory. The resulting hydrodynamic forces and wave-induced motions of a structure are computed, with which the effects of body motions on the local steady forces are properly evaluated. In the pressure-integration method, spatial derivatives of the velocity potential and the wave elevation at the waterline must be computed; which is successfully performed with the 9-point isoparametric representation for the surface geometry and velocity potential. Validity and numerical accuracy of the present method are confirmed by comparing the sum of local steady forces with the drift force computed by the far-field method.

Experiments are also carried out using 64 identical circular cylinders with horizontal base, arranged in a periodic array with 4 rows and 16 columns. Results of the steady wave forces measured at 6 selected positions are compared with corresponding numerical results. Good agreement is found between computed and measured results. Some characteristics of the local steady forces are noted, which are markedly different depending on the position of the cylinder in the array.

FORMULATION AND SECOND-ORDER FORCES

We consider the interactions of plane regular incident waves with a large floating structure. As shown in Fig. 1, the structure considered here comprises a thin upper deck and a large number of buoyancy columns which are identical and equally spaced. The geometry of an elementary column is a truncated circular cylinder with radius a and draft d. The centerlines of adjacent cylinders are separated by a distance $2s$ in both x- and y-axes of a Cartesian coordinate system. Here o-xyz is the body-fixed coordinate system with the origin placed at the center of gravity (G). In steady-state equilibrium, the position of G is supposed to be at $(0,\, 0,\, z_G)$ in a space-fixed coordinate system O-XYZ, where $Z = 0$ is taken as the undisturbed free surface and the Z-axis is positive vertically downward.

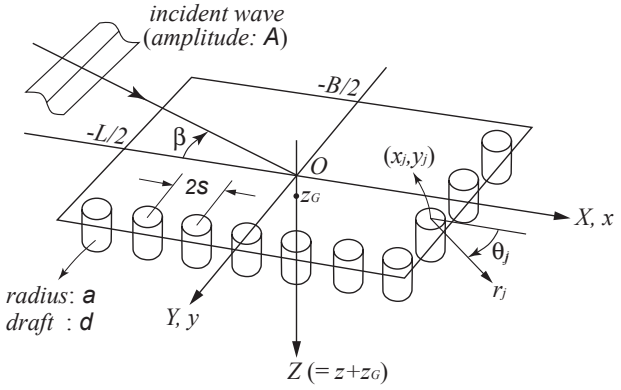

Fig. 1 Coordinate system and notations

The structure is allowed to move with unsteady motions of six degrees of freedom in response to the wave excitation. The vectors of the translational and rotational motions are denoted by $\boldsymbol{\xi}(t)$ and $\boldsymbol{\alpha}(t)$, respectively, and the magnitudes of these motions are assumed to be small. Then the vector of local displacement at a point on the body surface can be expressed as

$$\boldsymbol{\Xi}(t) = \boldsymbol{\xi}(t) + \boldsymbol{\alpha}(t) \times \boldsymbol{r}, \tag{1}$$

where $\boldsymbol{r} = (x,\, y,\, z)$ represents the position vector in the body-fixed reference frame.

Under the assumption of incompressible and inviscid flow with irrotational motion, we introduce the velocity potential, Φ, satisfying the Laplace equation. Assuming weak nonlinearities, the velocity potential and the motion vectors can be written as a perturbation series with respect to a small parameter ϵ, which is usually taken as the wave slope:

$$\left.\begin{aligned} \Phi &= \epsilon\, \Phi^{(1)} + \epsilon^2 \Phi^{(2)} + O(\epsilon^3), \\ \boldsymbol{\xi} &= \epsilon\, \boldsymbol{\xi}^{(1)} + \epsilon^2 \boldsymbol{\xi}^{(2)} + O(\epsilon^3), \\ \boldsymbol{\alpha} &= \epsilon\, \boldsymbol{\alpha}^{(1)} + \epsilon^2 \boldsymbol{\alpha}^{(2)} + O(\epsilon^3). \end{aligned}\right\} \tag{2}$$

Given the above quantities, the hydrodynamic pressure will be computed. Then the wave force on a body can be obtained by integrating the pressure multiplied by unit normal vector over the instantaneous wetted body surface, say $S(t)$.

Using (2) and Taylor's expansion for both the pressure and unit normal vector on $S(t)$ with respect to the mean body surface, S_B, the wave forces on a body can be expressed in a perturbation series. Details of the derivation can be found in, for example, Ogilvie (1983) and Kim & Yue (1990). The result can be summarized as follows:

$$\boldsymbol{F} = \boldsymbol{F}^{(0)} + \epsilon\, \boldsymbol{F}^{(1)} + \epsilon^2 \boldsymbol{F}^{(2)} + O(\epsilon^3), \tag{3}$$

where

$$\boldsymbol{F}^{(0)} = -\rho g V \boldsymbol{k}, \tag{4}$$

$$\boldsymbol{F}^{(1)} = \rho \iint_{S_B} \frac{\partial \Phi^{(1)}}{\partial t} \boldsymbol{n}\, dS - \rho g \iint_{S_B} \Xi_3^{(1)} n_3 \boldsymbol{k}\, dS, \tag{5}$$

$$\boldsymbol{F}^{(2)} = \rho \iint_{S_B} \frac{\partial \Phi^{(2)}}{\partial t} \boldsymbol{n}\, dS - \rho g \iint_{S_B} \Xi_3^{(2)} n_3 \boldsymbol{k}\, dS + \boldsymbol{F}_q^{(2)}, \tag{6}$$

$$\begin{aligned} \boldsymbol{F}_q^{(2)} = {} & \frac{1}{2}\rho \iint_{S_B} \left|\nabla \Phi^{(1)}\right|^2 \boldsymbol{n}\, dS - \frac{1}{2}\rho g \oint_{C_B} \left\{\zeta_R^{(1)}\right\}^2 \boldsymbol{n}\, d\ell \\ & + \rho \iint_{S_B} \boldsymbol{\Xi}^{(1)} \cdot \nabla\Big(\frac{\partial \Phi^{(1)}}{\partial t}\Big) \boldsymbol{n}\, dS + \boldsymbol{\alpha}^{(1)} \times \boldsymbol{F}^{(1)} \\ & - \rho g \iint_{S_B} \alpha_3^{(1)} \big(\alpha_1^{(1)} x + \alpha_2^{(1)} y\big) n_3 \boldsymbol{k}\, dS. \end{aligned} \tag{7}$$

Here $\zeta_R^{(1)}$ in (7) denotes the first-order relative wave elevation given by

$$\zeta_R^{(1)} = \frac{1}{g} \frac{\partial \Phi^{(1)}}{\partial t}\bigg|_{Z=0} - \Xi_3^{(1)}, \tag{8}$$

which must be evaluated along the mean waterline C_B; ρ is the fluid density; g is the gravitational acceleration; V is the displacement volume; $\boldsymbol{n}$ is the unit normal vector directing into the fluid from the mean body surface S_B; $\boldsymbol{\Xi}^{(1)} = \boldsymbol{\xi}^{(1)} + \boldsymbol{\alpha}^{(1)} \times \boldsymbol{r}$ and thus $\Xi_3^{(1)} = \xi_3^{(1)} + \alpha_1^{(1)} y - \alpha_2^{(1)} x$; $\boldsymbol{k}$ is the unit vector in the z-direction of the space-fixed coordinate axes.

The present paper is concerned with time-averaged steady forces, which can be computed only from $\boldsymbol{F}_q^{(2)}$ containing only quadratic products of first-order quantities.

The corresponding expressions for the moment about the center of gravity can be obtained in a similar form. The second-order term to be computed from quadratic products of first-order quantities, which is denoted as $\boldsymbol{M}_q^{(2)}$, may be computed by

$$\begin{aligned} \boldsymbol{M}_q^{(2)} = {} & \frac{1}{2}\rho \iint_{S_B} \left|\nabla \Phi^{(1)}\right|^2 \boldsymbol{r} \times \boldsymbol{n}\, dS - \frac{1}{2}\rho g \oint_{C_B} \left\{\zeta_R^{(1)}\right\}^2 \boldsymbol{r} \times \boldsymbol{n}\, d\ell \\ & + \rho \iint_{S_B} \boldsymbol{\Xi}^{(1)} \cdot \nabla\Big(\frac{\partial \Phi^{(1)}}{\partial t}\Big) \boldsymbol{r} \times \boldsymbol{n}\, dS + \boldsymbol{\alpha}^{(1)} \times \boldsymbol{M}^{(1)} \\ & - \rho g \iint_{S_B} \alpha_3^{(1)} \big(\alpha_1^{(1)} x + \alpha_2^{(1)} y\big) \boldsymbol{r} \times \boldsymbol{n}\, dS. \end{aligned} \tag{9}$$

The first-order motions, $\boldsymbol{\xi}^{(1)}$ and $\boldsymbol{\alpha}^{(1)}$, follow from the equations of motions based on Newton's second law, for which the first-order hydrodynamic force and moment must be computed.

SOLUTION OF FIRST-ORDER PROBLEM

The first-order quantities are assumed to be time-harmonic with circular frequency of the incident wave, ω, and are expressed

as

$$\Phi^{(1)} = \mathrm{Re}\Big[\, \frac{gA}{i\omega}\, \phi(x,y,z)\, e^{i\omega t} \Big], \tag{10}$$

$$\xi_k^{(1)} = \mathrm{Re}\Big[\, AX_k\, e^{i\omega t} \Big], \quad \alpha_k^{(1)} = \mathrm{Re}\Big[\, \frac{A}{a}\, X_{k+3}\, e^{i\omega t} \Big], \tag{11}$$

where A is the amplitude of the incident wave, and a is the radius of an elementary column which is used as the representative length scale for nondimensionalization. Note that $\phi(x,y,z)$ and X_j $(j = 1 \sim 6)$ are expressed as nondimensional quantities.

When solving the boundary-value problem with the free surface, it is convenient to use a space-fixed coordinate system. In the mean position of a body oscillating with a constant circular frequency, the body-fixed coordinate system coincides with one fixed in space except for the vertical shift of $z = z_G$. Therefore, in the analysis to follow, (x,y,z) will be used as the space-fixed coordinates.

The spatial part of the velocity potential, $\phi(x,y,z)$, can be decomposed in the form

$$\phi = \phi_I + \phi_S - K\sum_{k=1}^{6} X_k \big\{\, \phi_k + \varphi_k \,\big\}, \tag{12}$$

where $K = \omega^2 a/g$ is the nondimensional wavenumber.

ϕ_I and ϕ_S are the incident-wave and scattering potentials, respectively, and the sum, $\phi_I + \phi_S \equiv \phi_D$, is referred to as the diffraction potential. For plane waves propagating in the direction with angle β relative to the positive x-axis, ϕ_I is given by

$$\phi_I = \frac{\cosh k_0(z-h)}{\cosh k_0 h}\, e^{-ik_0(x\cos\beta + y\sin\beta)}, \tag{13}$$

where k_0 is the solution of $k_0 \tanh k_0 h = K$, and h denotes the constant water depth, nondimensionalized in terms of a.

In the radiation problem, ϕ_k in (12) denotes the velocity potential of a single body oscillating in the k-th mode (with no interactions among cylinders) and φ_k represents the remaining part of the potential due to hydrodynamic interactions with radiated and scattered waves by the other cylinders.

Therefore the boundary conditions to be satisfied on the mean body surface, S_B, are given as

$$\frac{\partial \phi_D}{\partial n} = 0, \quad \frac{\partial \phi_k}{\partial n} = n_k, \quad \frac{\partial \varphi_k}{\partial n} = 0, \tag{14}$$

where $\boldsymbol{n} = (n_1, n_2, n_3)$ and $\boldsymbol{r} \times \boldsymbol{n} = (n_4, n_5, n_6)$.

Solutions satisfying (14) and other free-surface and radiation conditions may be obtained by using Kagemoto & Yue's interaction theory (1986). To obtain expressions valid near the j-th cylinder (see Fig. 1) using the interaction theory, we will use a local cylindrical coordinate system (r_j, θ_j, z), with the origin placed at the center of the j-th cylinder, $(x_j, y_j, 0)$. Namely, $x = x_j + r_j\cos\theta_j$ and $y = y_j + r_j \sin\theta_j$ will be substituted.

The expressions of the velocity potentials by the interaction theory, appropriate for the present analyses, may be found in Kashiwagi (1998), and the results are summarized as follows:

$$\phi_D^j = \Big(\big\{a^j\big\}^T + \sum_{\substack{i=1\\ i\neq j}}^{N_B} \big\{A_S^i\big\}^T \big[\, T_{ij} \big] \Big) \big\{\psi_D^j\big\}, \tag{15}$$

$$\phi_k^j = \big\{\mathcal{R}_k^j\big\}^T \big\{\psi_S^j\big\}, \tag{16}$$

$$\varphi_k^j = \sum_{\substack{i=1\\ i\neq j}}^{N_B} \Big(\big\{\mathcal{R}_k^j\big\}^T + \big\{A_k^i\big\}^T \Big) \big[\, T_{ij} \big] \big\{\psi_D^j\big\}, \tag{17}$$

where

$$\big\{\psi_D^j\big\} = \big\{\psi_I^j\big\} + \big[\, B_j \,\big] \big\{\psi_S^j\big\}. \tag{18}$$

Here $\big\{\psi_I^j\big\}$ and $\big\{\psi_S^j\big\}$ in (18) are the vectors of the "generalized" incident-wave and scattering potentials, respectively, defined as

$$\big\{\psi_I^j\big\} = \left\{ \begin{array}{l} Z_0(z)\, J_p(k_0 r_j)\, e^{-ip\theta_j} \\ Z_n(z)\, I_p(k_n r_j)\, e^{-ip\theta_j} \end{array} \right\}, \tag{19}$$

$$\big\{\psi_S^j\big\} = \left\{ \begin{array}{l} Z_0(z)\, H_m^{(2)}(k_0 r_j)\, e^{-im\theta_j} \\ Z_n(z)\, K_m(k_n r_j)\, e^{-im\theta_j} \end{array} \right\}, \tag{20}$$

where

$$Z_0(z) = \frac{\cosh k_0(z-h)}{\cosh k_0 h}, \quad Z_n(z) = \frac{\cos k_n(z-h)}{\cos k_n h}, \tag{21}$$

and k_n $(n = 1, 2, \cdots)$ are solutions of $k_n \tan k_n h = -K$, giving the wavenumbers of evanescent wave modes. The number of terms in the θ-direction, p and m in (19) and (20), must be taken as 0, ± 1, ± 2, $\cdots$.

The coefficient vector of the incident wave, $\big\{a^j\big\}$, can be explicitly given by expressing (13) in terms of a local cylindrical coordinate system. Meanwhile, $\big[\, T_{ij} \big]$ is the coordinate transformation matrix, relating $\big\{\psi_I^i\big\}$ with $\big\{\psi_S^j\big\}$, which can be given by Graf's addition theorem for Bessel functions. N_B denotes the number of total cylinders.

The vector $\big\{\mathcal{R}_k^j\big\}$ in (16) can be numerically obtained by solving the radiation problem for a single body. Likewise, the matrix $\big[\, B_j \,\big]$ in (18) can be obtained by solving the diffraction problem for a single body, with each component of (19) regarded as an incident-wave velocity potential. For these numerical computations, a higher-order boundary element method using 9-point isoparametric elements is adopted in the present paper.

Other unknown vectors representing wave interactions, $\big\{A_S^i\big\}$ in (15) and $\big\{A_k^i\big\}$ in (17), are determined by Kagemoto & Yue's interaction theory.

Once the velocity potentials are determined, it is straightforward to compute the first-order forces acting in the k-th direction; those are expressed in a nondimensional form as follows:

$$\left. \begin{array}{l} F_k^{(1)} = \mathrm{Re}\big[\, \rho g A\, a^2\, \mathcal{F}_k\, e^{i\omega t} \,\big], \\ M_k^{(1)} = \mathrm{Re}\big[\, \rho g A\, a^3\, \mathcal{F}_{k+3}\, e^{i\omega t} \,\big], \end{array} \right\} \tag{22}$$

where

$$\mathcal{F}_k^j = E_k^j + \sum_{\ell=1}^{6} X_\ell \big\{\, KF_{k\ell}^j - C_{k\ell}^j \,\big\}, \tag{23}$$

$$E_k^j = \Big(\big\{a^j\big\}^T + \sum_{\substack{i=1\\ i\neq j}}^{N_B} \big\{A_S^i\big\}^T \big[\, T_{ij} \big] \Big) \big\{e_k^j\big\}, \tag{24}$$

$$F_{k\ell}^j = f_{k\ell}^j - \sum_{\substack{i=1\\ i\neq j}}^{N_B} \Big(\big\{\mathcal{R}_k^i\big\}^T + \big\{A_k^i\big\}^T \Big) \big[\, T_{ij} \big] \big\{e_k^j\big\}. \tag{25}$$

Here $f_{k\ell}^j$ in the radiation force and $\big\{e_k^j\big\}$ in the diffraction and interaction forces are fundamental hydrodynamic forces of a single body, which can be computed by

$$\left. \begin{array}{l} f_{k\ell}^j = -\displaystyle\iint_{S_B} \phi_\ell^j\, n_k^j\, dS, \\ \big\{e_k^j\big\} = \displaystyle\iint_{S_B} \big\{\psi_D^j\big\}\, n_k^j\, dS, \end{array} \right\} \tag{26}$$

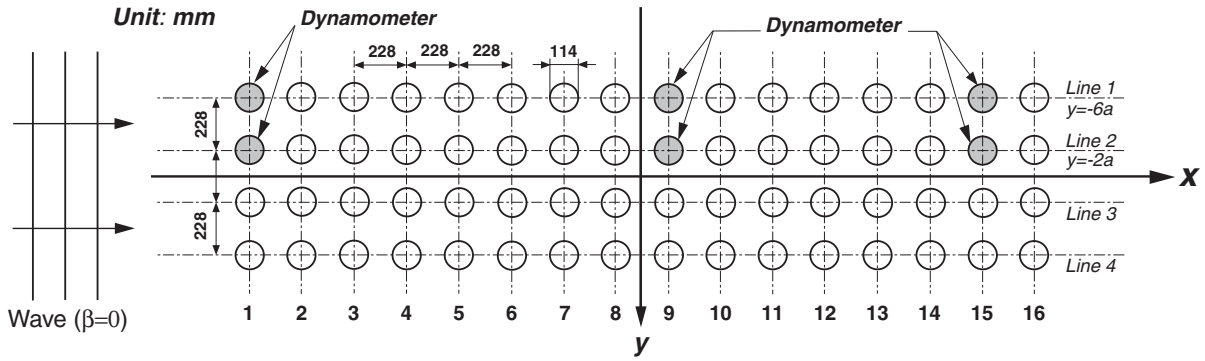

Fig. 2 Experimental model: arrangement of 64 truncated circular cylinders fixed in head waves

with n_k^j being the k-th component of unit normal vector on the j-th cylinder.

$C_{k\ell}^j$ appearing in (23) denotes the restoring force coefficients; nonzero values among these coefficients for a vertical circular cylinder are summarized as follows:

$$\left.\begin{aligned} C_{33}^j &= \pi, \\ C_{44}^j &= \pi\Big\{ y_j^2 + \frac{1}{4} - d\left(\frac{d}{2} - z_G\right)\Big\}, \\ C_{55}^j &= \pi\Big\{ x_j^2 + \frac{1}{4} - d\left(\frac{d}{2} - z_G\right)\Big\}, \\ C_{34}^j &= C_{43}^j = \pi y_j, \quad C_{35}^j = C_{53}^j = -\pi x_j, \\ C_{45}^j &= C_{54}^j = -\pi x_j y_j. \end{aligned}\right\} \tag{27}$$

Having determined the hydrodynamic and hydrostatic forces, the complex amplitude X_k defined in (11) will be determined by solving the motion equations of a structure with N_B buoyancy cylinders.

The steady wave forces and moments can be obtained by taking time average over one period of $\boldsymbol{F}_q^{(2)}$ given as (7) and $\boldsymbol{M}_q^{(2)}$ given as (9), respectively.

As shown in (10), (11) and (22), the time-dependent part of all first-order quantities are expressed as $e^{i\omega t}$. Therefore the time average can be easily computed by means of the following formula:

$$\overline{\mathrm{Re}\big[\, A\, e^{i\omega t}\,\big]\,\mathrm{Re}\big[\, B\, e^{i\omega t}\,\big]} = \frac{1}{2}\,\mathrm{Re}\big[\, A\, B^*\,\big], \tag{28}$$

where the overbar means the time average to be taken and the asterisk denotes the complex conjugate.

As a special case of (7) and (9), when the body motions are completely restrained, calculation formulae for the time-averaged steady forces and moments become much simpler, including only the diffraction components. For instance, the nondimensional expression for the steady force, $\bar{\boldsymbol{F}}$, can be given by

$$\frac{\bar{\boldsymbol{F}}}{\frac{1}{2}\rho g A^2 a} = \frac{1}{2}\left[\frac{1}{K}\iint_{S_B} |\,\nabla\phi_D\,|^2\,\boldsymbol{n}\,dS - \oint_{C_B} |\,\phi_D\,|^2\,\boldsymbol{n}\,d\ell\right]. \tag{29}$$

OUTLINE OF EXPERIMENTS

With the calculation method described in the preceding section, the effects of body motions on the steady forces can be taken into account. However, to check validity and performance of the calculation method for the diffraction problem first, motions were completely fixed in experiments.

As shown in Fig. 2, experiments were conducted in head waves ($\beta = 0^\circ$), using 64 equally-spaced truncated circular cylinders. The diameter ($D = 2a$) of an elementary cylinder is 114 mm. The separation distance between centerlines of adjacent cylinders, $2s$, was set equal to $2D$ in both x- and y-axes; that is, $s = D$. To see effects of the draft of cylinders on the wave interactions, two cases of $d = D$ and $d = 2D$ were tested, but only the results of $d = 2D$ will be presented in this paper, because there were no essential differences between the two cases.

The wave forces were measured by dynamometers at 6 different positions. As shown in Fig. 2, 16 columns are numbered from the upwave side. By symmetry, the lines of $y = \pm 2a$ are called the inside and the lines of $y = \pm 6a$ are called the outside. Then the positions of measured cylinders are distinguished with the column number and the inside or outside line.

The steepness of regular waves (the ratio of wave height with wave length, H/λ) was set approximately equal to 1/50. The circular frequency ω of incident waves was varied in the range of $Ks = \omega^2 s/g = 0.2 \sim 1.6$. Measured data were analyzed using an ordinary Fourier analysis, from which the steady force in the x-axis was obtained.

RESULTS AND DISCUSSION

Outline of Numerical Computations

As the first step of numerical computations, the boundary-value problems for a single cylinder were solved by the boundary element method using 9-point quadratic representations for both the surface geometry and velocity potential. The number of panels over one quarter of the submerged surface was 40, and in this case the number of total unknowns (velocity potentials at nodes) was 177.

In computing the wave interactions, the number of Fourier series in the θ-direction (M) and of evanescent wave mode (N) must be finite. In the present paper, $M = 5$ and $N = 3$ are chosen after convergence check for $Ks = 1.0$, $\beta = 0^\circ$, and $h = 3d$, for which five decimals absolute accuracy has been achieved.

The number of total unknowns for $M = 5$, $N = 3$, and $N_B = 64$ is $(2M + 1) \times (N + 1) \times N_B = 2816$. The computation time in this case will be very long, if computations must be carried out at many frequencies for higher resolution. Therefore, double symmetries with respect to x- and y-axes are exploited, which can reduce the number of unknowns to 1/4 (*i.e.* 2816/4=704).

The spatial derivatives of the velocity potential over the submerged surface, S_B, which are needed in computing the second-order steady forces by the present method, are evaluated using 2-

Table 1 Steady forces in surge, sway, and yaw on a structure with 64 circular cylinders arranged periodically in the array of 4 rows and 16 columns, computed by the far-field method and the pressure integration method. ($d = 2D$, $s = D$, $h = 7.5\,d$, $\beta = 30°$)

By Far-Field Method (Momentum-Conservation Principle)

	Diffraction Problem			Including Motion Effects		
Ks	FX	FY	MZ	FX	FY	MZ
0.50	0.05413	0.00876	0.00412	0.14638	0.01407	-0.10189
1.00	0.08821	0.04253	0.02977	0.08946	0.04258	0.03098
1.50	1.6217	0.08032	-0.00668	1.6218	0.08030	-0.00606
1.75	3.9364	0.27782	0.40703	3.9369	0.27766	0.40795
2.00	3.2052	0.70410	-0.26574	3.2048	0.70387	-0.26517
2.50	0.98615	0.50644	-0.37112	0.98633	0.50677	-0.37146

By Near-Field Method (Direct Pressure Integration)

	Diffraction Problem			Including Motion Effects		
Ks	FX	FY	MZ	FX	FY	MZ
0.50	0.05576	0.00874	0.00343	0.17035	0.01336	-0.10203
1.00	0.08868	0.04209	0.02975	0.08997	0.04213	0.03099
1.50	1.6222	0.08027	-0.00664	1.6223	0.08025	-0.00602
1.75	3.9368	0.27791	0.40708	3.9373	0.27775	0.40799
2.00	3.2056	0.70419	-0.26571	3.2052	0.70396	-0.26513
2.50	0.98646	0.50627	-0.37130	0.98664	0.50661	-0.37164

D quadratic isoparametric representations for the velocity potential and coordinates (x, y, z). The line integral along the waterline, C_B, which is also needed in the pressure-integration method, is evaluated using 1-D quadratic isoparametric representations for the velocity potential at $z = 0$ and coordinates (x, y).

Total Drift Force on 64 Cylinders

Based on the momentum-conservation principle, Kashiwagi (2000) developed a calculation method (the so-called far-field method) for computing the drift forces in the horizontal plane and the drift yaw moment. Although this far-field method gives only the total force on the structure, accurate results can be expected, because all necessary integrations on a control surface located far from the structure are analytically performed. Therefore, to check numerical accuracy of the present method, the summation of the local steady forces on 64 cylinders was compared with independent results by the far-field method.

Figure 3 is taken from Kashiwagi (2000), showing the results computed by the far-field method for the surge drift force in head waves. Corresponding results computed by the present method are shown in Fig. 4, which is in virtually perfect agreement with Fig. 3 except for very small difference near $Ks = 1.24$.

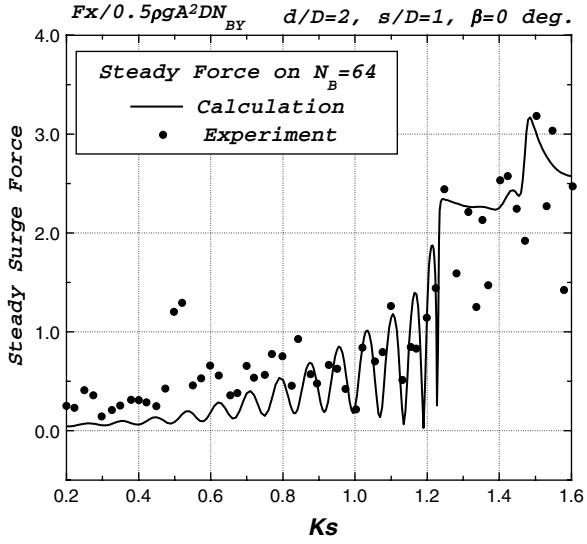

Fig. 3 Total wave drift force on 64 circular cylinders, computed by the far-field method

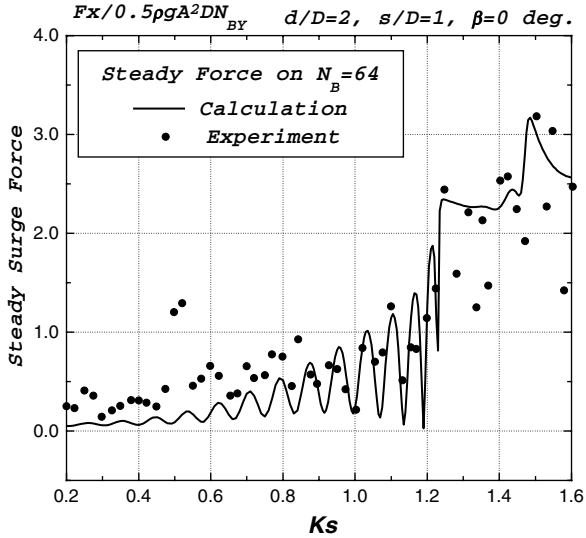

Fig. 4 Total wave drift force on 64 circular cylinders, computed by the pressure-integration method

For the case of freely oscillating in response to the wave excitation, comparison of the results is shown in Table 1 at some wavenumbers. To show the results of the steady sway force (FY) and yaw moment (MZ), computations were performed for $\beta = 30^\circ$, and other geometrical parameters are the same as Figs. 3 and 4. The center of gravity was assumed to be on the water plane and the radii of gyration in roll, pitch, and yaw modes were set to $0.25B$, $0.25L$, and $0.25L$, respectively, with B and L being the breadth and length, respectively, of the structure composed of 64 cylinders.

We can see from Table 1 that very good agreement exists between the far-field method and the present method based on the direct pressure integration. For higher frequencies, the steady forces and moment become large and the yaw moment changes the sign abruptly around $Ks = 1.7$, but major contributions stem from the diffraction component. This is because the structure considered here is large compared to the wavelength of the incident wave and thus the wave-induced motions are relatively small for higher frequencies. Notwithstanding small values of motions, we can see that the effects of body motions are properly computed by the present method.

Comparison with Experiments

Having confirmed the validity and accuracy of the present method, let us investigate the local steady forces on elementary cylinders by comparing with experimental measurements.

Figure 5 shows the steady surge force on the cylinder located at Column No. 1 along the inside line (see Fig. 2). Likewise, Fig. 6 shows the results on the cylinder at Column No. 1 along the outside line. In the frequency range less than $Ks \simeq 1.24$, we can see regular fluctuation with increasing amplitude, which may be due to the effects of wave reflection from downwave cylinders. On the other hand, at frequencies higher than $Ks \simeq 1.24$, the variation pattern changes and the steady force becomes positive.

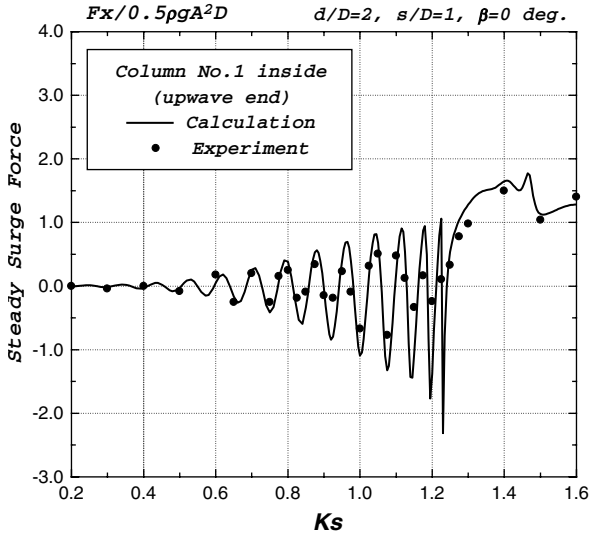

Fig. 5 Steady surge force on the cylinder at Column No. 1 along the inside line

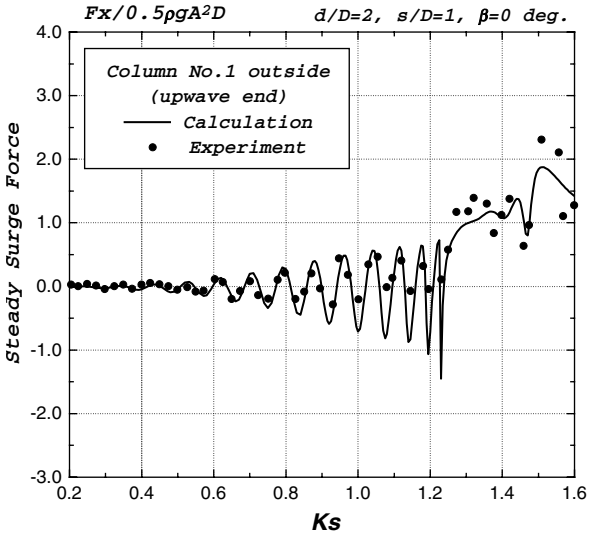

Fig. 6 Steady surge force on the cylinder at Column No. 1 along the outside line

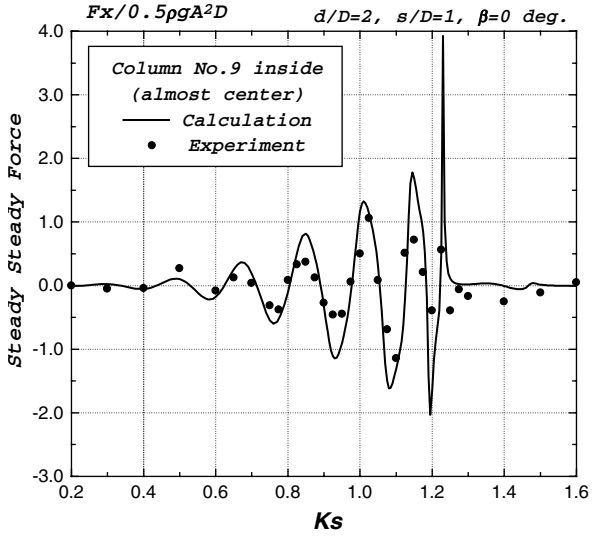

Fig. 7 Steady surge force on the cylinder at Column No. 9 along the inside line

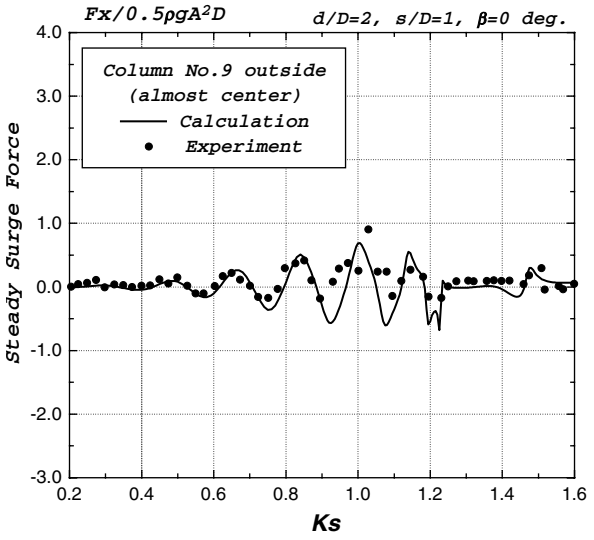

Fig. 8 Steady surge force on the cylinder at Column No. 9 along the outside line

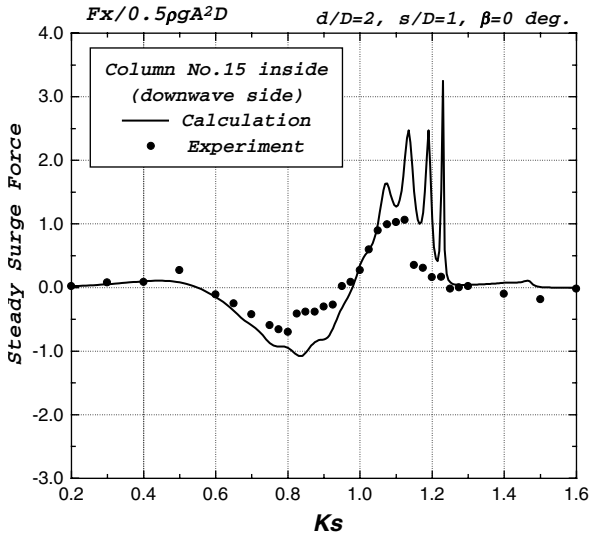

Fig. 9 Steady surge force on the cylinder at Column No. 15 along the inside line

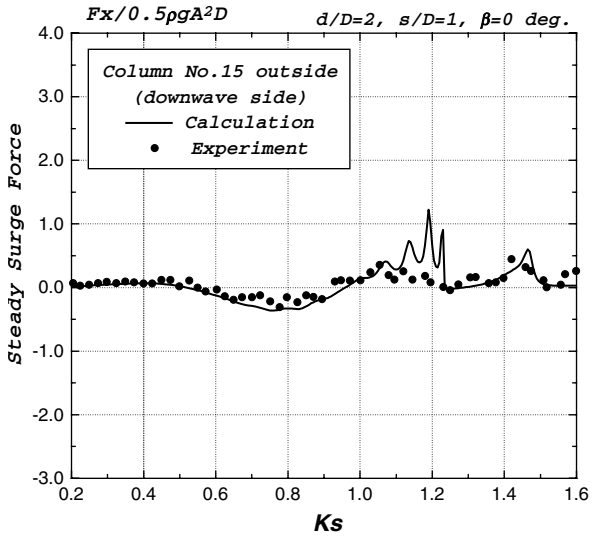

Fig. 10 Steady surge force on the cylinder at Column No. 15 along the outside line

This implies that large part of the incident wave is reflected by the cylinders placed near the upwave end, and that the total drift force (shown in Figs. 3 and 4) is determined almost by the local steady forces acting on upwave cylinders. (The latter conjecture will be endorsed by observing the results on downwave cylinders, shown in Figs. 7–10.) According to Maniar & Newman (1997), $Ks = 1.24$ corresponds approximately to a near trapped-mode frequency of Neumann type, around which linear wave forces become large and change drastically.

Comparison between Fig. 5 and Fig. 6 reveals that the amplitude of fluctuation at lower frequencies is larger at the inside than that at the outside. Although the fluctuation amplitude just below the near trapped-mode frequency is not so large in measured results, the overall agreement between computed and measured results is satisfactory.

Figures 7 and 8 are the results of the steady surge force on the cylinders at Column No. 9. It is clearly shown that the steady force at the inside (Fig. 7) is much larger in amplitude than that at the outside (Fig. 8). This implies that the wave interactions are intensified inside the array of a large number of cylinders. By comparison with Figs. 5 and 6, we can see that variation of the steady force with respect to Ks becomes mild for lower frequencies. On the other hand, at frequencies higher than $Ks \simeq 1.24$, the steady forces at Column No. 9 are almost zero. Including these characteristics, computed results are in good agreement with measured results.

Figures 9 and 10 show the steady surge force on cylinders at Column No. 15 (the second column from the most downwave side). We can see again that the steady force at the inside is larger than that at the outside and the variation with respect to Ks becomes further mild. The present computations predict a spike-like rapid change just below the near trapped-mode frequency, but that is not clear in measured results; which may be attributed to a decay due to viscous effects.

CONCLUDING REMARKS

A calculation method based on the direct pressure integration was presented for computing the steady force and moment on a column-supported large floating structure. This method enables us to compute the local steady forces on each of a large number of columns. Although the steady forces are dominated by the diffraction component for practical frequencies because of large scale of the structure, the effects of wave-induced motions of the structure are also taken into account. The pressure on the wetted surface of each column was computed by the wave-interaction theory which is exact in the framework of the linear potential theory.

Validity and numerical accuracy of the present method were confirmed by comparing the sum of local steady forces on 64 vertical cylinders with the wave drift force computed by the far-field method based on the momentum-conservation principle.

Concerning the characteristics of the local steady forces on each cylinder, computed results were compared with measured ones using 64 vertical cylinders arranged in 4 rows and 16 columns, through which we observed the followings:

1) The overall agreement is very good, considering that the steady forces are second-order small quantities in the wave amplitude.
2) The steady force on each column can be negative, though the total force summing up the local forces of all columns is definitely positive.
3) At the upwave side, the variation of the steady force is rapid in the frequency range lower than the near trapped-mode frequency, but this variation becomes mild as the position of a cylinder goes downstream.
4) For higher frequencies than the near trapped-mode frequency, the local steady forces on upwave cylinders become positive and large, dominating the total drift force on the whole structure.
5) The steady force on a cylinder along the inside line in the array is larger than that on a cylinder along the outside line in the variation amplitude with respect to the frequency.

ACKNOWLEDGMENTS

Experiments in this study have been conducted as a part of the master thesis of Mr. S. Yoshida, in the Interdesciplinary Graduate School of Engineering Sciences, Kyushu University. The

author is thankful for his contribution. Thanks are also extended to Mr. M. Inada for his help in preparation of experiments.

REFERENCES

Kagemoto, H and Yue, DKP (1986). "Interactions among Multiple Three-Dimensional Bodies in Water Waves: An Exact Algebraic Method", *Journal of Fluid Mechanics*, Vol 166, pp 189–209.

Kashiwagi, M (1998). "Hydrodynamic Interactions among a Great Number of Columns Supporting a Very Large Flexible Structure", *Proc 2nd Intl Conf on Hydroelasticity*, Fukuoka, pp 165–176.

Kashiwagi, M (1999). "Research on Hydroelastic Responses of VLFS: Recent Progress and Future Work", *Proc 9th Intl Offshore and Polar Engineering Conf*, Brest, Vol 1, pp 17–26.

Kashiwagi, M (2000). "Wave Drift Force and Moment on a VLFS Supported by a Great Number of Floating Columns", *Proc 10th Intl Offshore and Polar Engineering Conf*, Seattle, Vol 1, pp 49–56.

Kim, MH and Yue, DKP (1990). "The Complete Second Order Diffraction Solution for an Axisymmetric Body, Part 2. Bichromatic Incident Waves and Body Motions", *Journal of Fluid Mechanics*, Vol 211, pp 557–593.

Maniar, HD and Newman, JN (1997). "Wave Diffraction by a Long Array of Cylinders", *Journal of Fluid Mechanics*, Vol 339, pp 309–330.

Ogilvie, TF (1983). "Second Order Hydrodynamic Effects on Ocean Platforms", *Intl Workshop on Ship and Platform Motion*, Berkeley, pp 205–265.